Surface oxides on Pd(111): STM and density functional calculations

J. Klikovits,[1] E. Napetschnig,[1] M. Schmid,[1,*] N. Seriani,[2] O. Dubay,[2] G. Kresse,[2] and P. Varga[1]
[1]*Institut für Allgemeine Physik, Technische Universität Wien, A-1040 Wien, Austria*
[2]*Computational Materials Physics, Universität Wien, A-1090 Wien, Austria*
(Received 2 May 2007; published 10 July 2007)

The formation of one-layer surface oxides on Pd(111) has been studied by scanning tunneling microscopy (STM) and density functional theory (DFT). Besides the Pd_5O_4 structure determined previously, structural details of six different surface oxides on Pd(111) will be presented. These oxides are observed for preparation in oxygen-rich conditions, approaching the thermodynamic stability limit of the PdO bulk oxide at an oxygen chemical potential of −0.95 to −1.02 eV (570–605 K, 5×10^{-4} mbar O_2). Sorted by increasing oxygen fraction in the primitive unit cell, the stoichiometry of the surface oxides is Pd_5O_4, Pd_9O_8, $Pd_{20}O_{18}$, $Pd_{23}O_{21}$, $Pd_{19}O_{18}$, Pd_8O_8, and $Pd_{32}O_{32}$. All structures are one-layer oxides, in which oxygen atoms form a rectangular lattice, and all structures follow the same rules of favorable alignment of the oxide layer on the Pd(111) substrate. DFT calculations were used to simulate STM images as well as to determine the stability of the surface oxide structures. Simulated and measured STM images are in excellent agreement, indicating that the structural models are correct. Since the newly found surface oxides are clearly less stable than Pd_5O_4, we conclude that Pd_5O_4 is the only thermodynamically stable phase, whereas all newly found structures are only kinetically stabilized. We also discuss possible mechanisms for the formation of these oxide structures.

DOI: 10.1103/PhysRevB.76.045405 PACS number(s): 68.47.Gh, 68.37.Ef, 68.35.Md

I. INTRODUCTION

Surfaces of transition metals used in catalysis undergo oxidation under realistic catalytic conditions, and oxide formation dramatically changes their properties. It was found that in many cases catalytic activity can be attributed to oxides rather than to pure metal surfaces.[1,2] Besides the formation of superstructures by adsorbed oxygen and bulk oxides, oxidation of a metal surface often leads to complex two-dimensional structures, which are different from the metal as well as from the respective bulk oxides.[3–13] These so-called "surface oxides" are either only kinetically stabilized[6] or represent the thermodynamically stable structure for a certain oxygen chemical potential range.[4,9] Surface oxides can also act as an oxygen reservoir for oxidation reactions.[14,15] Oxygen exposure to Pd(111) results in the formation of an ordered (2×2) oxygen superstructure with a coverage of 0.25 monolayer (ML) (Refs. 16–19) and surface oxides for higher oxygen chemical potentials[3,4,10]—i.e., oxygen pressures above 5×10^{-6} mbar at 300 °C. The "$\sqrt{6}$" structure, which was identified as a Pd_5O_4 surface oxide, has already been solved by a combination of experimental and theoretical methods.[4] It was found that this Pd_5O_4 surface oxide is thermodynamically stable for a chemical potential between −1.15 and −1 eV.[10] The primitive unit cell of this one-layer surface oxide is quadratic, and it has side lengths of 0.674 nm, which is $\sqrt{6}$ times the nearest-neighbor distance of Pd. One diagonal of the primitive unit cell runs parallel to a close-packed substrate row, and its length is incommensurate with the substrate, whereas the second diagonal is commensurate with the substrate. Oxidation of the Pd(111) surface using NO_2 leads to the formation of a surface that is covered by various surface oxides including the $\sqrt{6}$ structure.[3] By using molecular oxygen instead of NO_2 for oxidizing the Pd(111) surface as in Ref. 4 and in the current work, a similar surface can be prepared and the same surface oxides are observed by scanning tunneling microscopy (STM) for high oxygen chemical potential (approximately −1 eV). Since under these preparation conditions the oxidized Pd(111) surface is covered by small domains of at least seven different surface oxides, STM at high resolution is an adequate experimental method for determining the structures. Despite the fact that the electronic structure of a surface is probed by STM rather than the atomic arrangement, a comparison with the well-known Pd_5O_4 structure facilitates a correct interpretation of the STM images. For some of the newly found surface oxides, we observe structural similarities not only with Pd_5O_4, but also with $(\sqrt{5}\times\sqrt{5})R27°$ PdO on Pd(100).[5,13] The proposed models are confirmed by density-functional-theory- (DFT-) based calculations of STM images, and a phase diagram based on first-principles thermodynamics is presented.

II. EXPERIMENTAL AND COMPUTATIONAL METHODS

In our experiments we used two similar Pd(111) single crystals, cleaned by cycles of Ar^+ ion sputtering and subsequent annealing at 900 °C. No contaminants such as O, C, or S could be detected by Auger electron spectroscopy after these cycles. The surface was heated to the target temperature in oxygen and oxidized at 5×10^{-4} mbar O_2 at temperatures between 570 and 605 K for 10 min, which corresponds to an oxygen chemical potential between −0.95 and −1.02 eV. Cooling from the target temperature in oxygen gave similar results as cooling down at constant oxygen chemical potential. Some images were obtained on a 3-ML thin Pd layer on a partly oxidized Rh(111) single crystal, which has a rougher surface than Pd single crystals. Nevertheless, it exhibits the same surface oxides as on Pd(111) under similar oxidizing conditions.

STM measurements were done in an ultrahigh-vacuum (UHV) chamber with a base pressure of 5×10^{-11} mbar. No changes induced by the residual gas could be observed for the duration of the STM measurements. Images were taken

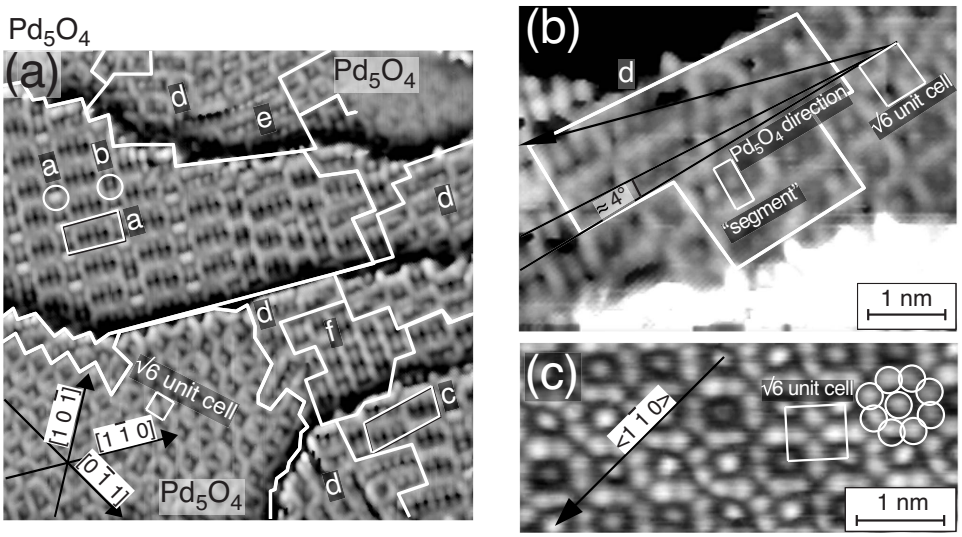

FIG. 1. STM images of a surface covered by various one-layer surface oxides (marked by letters *a*–*f*) grown on a 3-ML thin Pd film (a) overview (15 nm × 15 nm; −18 mV, 0.54 nA) with the unit cells of structures *a* and *c* marked, (b) close-up of an area covered by structure *d* and (c) atomically resolved image of an Pd_5O_4 area grown on Pd(111) (−1.8 mV, 4.38 nA, Pd is visible).

in constant current mode using the same instrument as in Ref. 4.

The calculations were performed using the Vienna ab-initio simulation package[20] (VASP) and the projector augmented-wave (PAW) method, in which the exact valence wave functions instead of pseudo-wave-functions, as in conventional pseudopotential calculations, are used.[21,22] An energy cutoff of 250 eV was employed. The PAW potentials applied in the present study were also used in Refs. 4 and 13. Brillouin zone integration was performed on Monkhorst-Pack grids roughly corresponding to a (16×16) grid in the (1×1) cell of clean Pd(111). All calculations presented here were performed with the generalized gradient approximations of Perdew and Wang (PW91).[23] The surface was modeled by a slab containing four to six metallic layers, of which the upper two were fully relaxed together with the oxide layer until the forces on the atoms became smaller than 0.02 eV/Å. Simulated STM images were calculated using the Tersoff-Hamann approach[24] considering states between the Fermi level ±0.2 eV. Thermodynamic stability of the structures was investigated by means of first-principles thermodynamics combining DFT total energies with thermodynamic data for the oxygen gas to calculate Gibbs free energies. Phonon contributions were neglected.[25,26]

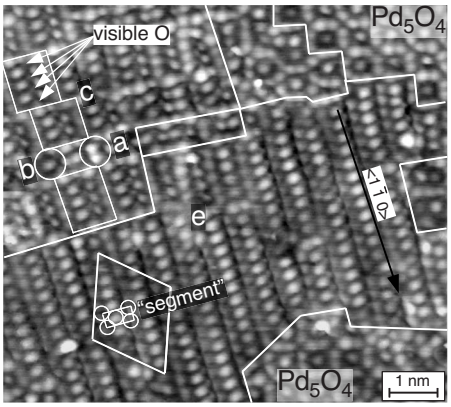

FIG. 2. Atomically resolved STM image of an oxidized Pd(111) surface covered by the surface oxides *a*, *b*, *c*, *e*, and Pd_5O_4 (−1.8 mV, 4.38 nA; Pd atoms in the "segment" are indicated by circles). The rhomb in the bottom left side is the $Pd_{32}O_{32}$ unit cell.

III. EXPERIMENTAL RESULTS

A. Pd_5O_4 structure

Figure 1 shows an STM image of the oxidized Pd(111) surface. Areas covered by the Pd_5O_4 surface oxide, which can be easily recognized by their characteristic "Persian carpet" pattern, are marked. We can distinguish between the commensurate and incommensurate directions in STM, since clear brightness variations are observed in STM only along the incommensurate direction. Therefore, we can use the Pd_5O_4 surface oxide to exactly determine the orientation of the Pd substrate on a fully oxide covered surface as is indicated in Figs. 1 and 2.

The characteristic "Persian carpet" pattern[4] can also be found on most monolayer-high islands formed by excess Pd, as was observed also in Ref. 3, whereas the rest of the surface is covered by various surface oxides as indicated in Fig. 3.

Concerning the structure of the Pd_5O_4 surface oxide, the oxygen atoms form a square lattice in which they avoid hollow positions with respect to the Pd(111) substrate. Pd atoms

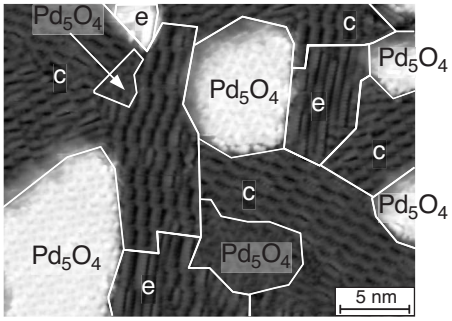

FIG. 3. STM image of a fully oxide covered Pd(111) surface (−0.5 V, 0.54 nA). Excess Pd forms monolayer-high islands during oxidation (bright areas). Islands are covered mainly by Pd_5O_4, whereas island-free parts are covered by various surface oxides.

are located in between the oxygen so that Pd atoms can be either twofold or fourfold oxygen coordinated. In the STM images, Pd is displayed much brighter than oxygen both in atomically resolved images [Fig. 1(c)] as well as in images without atomic resolution [Fig. 1(a)]. In images without atomic resolution, fourfold-oxygen-coordinated Pd is displayed as sharp, bright spots, whereas twofold-coordinated Pd is also bright, but blurred.[4,13]

B. Unit cells of the structures

Domains of various surface oxides cover the surface area in Fig. 1(a). Areas covered by these surface oxides are marked with letters *a*–*f*. The primitive unit cells are marked in areas *a* and *c*.

A large domain is covered by structures *a* and *b*. These two structures differ only in one position as indicated by circles in Fig. 1(a). In STM, we observe an elongated spot of exceptional brightness for structure *a* in a position where *b* appears rather dark. Both structures have the same rectangular unit cell. As determined from comparison with the Pd_5O_4 cell; the long side is parallel to a close-packed substrate direction and has a length of seven substrate nearest-neighbor distances. The short side has the same length as the diagonal of the Pd_5O_4 unit cell, which is four substrate row distances. Commensurability and an exact alignment parallel to a close-packed substrate direction are also indicated by the fact that no brightness variations between adjacent unit cells can be observed in STM, as was the case only for the commensurate direction of Pd_5O_4 (see Sec. III A). The quite similar structure *c* can be found in the lower right corner of Fig. 1(a). Obviously, it is composed of similar building blocks as *a* and *b*. As determined by STM, each building block is parallel to a close-packed substrate row and adjacent blocks are shifted by one substrate row distance. The primitive unit cell is a rhomboid as indicated in Fig. 1(a). Regarding commensurability, the same arguments as for structures *a* and *b* can be applied; thus, structure *c* is commensurate with the substrate.

In Fig. 1(b), we also observe rectangular structures with short sides of nearly the same length as the Pd_5O_4 unit cell (0.674 nm). The long sides of these rectangular structures are expanded by adding a variable number of "segments" to the Pd_5O_4 primitive unit cell, thereby forming chains of different length (structure *d*). As more of these segments are added, we observe that the resulting structure becomes differently orientated with respect to the substrate than Pd_5O_4. Rotation by $\approx 4°$ is already observed in STM if two segments are added as in Fig. 1(b). A stronger rotation can be observed in the atomically resolved STM image in Fig. 2, where a large number of these segments form structure *e*. These long chains run almost parallel to close-packed substrate rows. Compared to Pd_5O_4, the orientation with respect to the substrate has changed by almost 15°. Along the chains we measure a distance between adjacent bright atoms (Pd) of 0.3 nm and the distance between equivalent rows is roughly 0.63 nm, which is slightly less than the Pd_5O_4 unit cell length of 0.674 nm. We further observe brightness modulations along the chains and that long chains appear slightly wavy instead of running perfectly straight. Although the structure appears to be incommensurate in most of Fig. 2, in parts of the image a rather large commensurate cell can be found as indicated in Fig. 2. This unit cell is best described in a matrix notation as $\begin{pmatrix} 5 & -3 \\ 7 & 5 \end{pmatrix}$.

In Fig. 1(a) we also observe a small domain covered by structure *f* between Pd_5O_4 areas and the above-mentioned structures *a*, *b*, and *c*. A commensurate unit cell, which runs almost perpendicular to a close-packed substrate row, can be attributed to this transition structure. In matrix notation the unit cell is described as $\begin{pmatrix} 2 & -1 \\ 2 & 5 \end{pmatrix}$.

C. Determining the Pd positions

Comparing the observed pattern for the "$\sqrt{6}$" structure in Fig. 2 with the model from Ref. 4, one recognizes that Pd is the only visible species in the Pd_5O_4 areas. Despite the fact that Pd atoms do not appear at the same brightness due to different oxygen coordination and alignment with respect to the substrate, we assume that generally only Pd is visible in Fig. 2. Therefore, we determine the number of Pd atoms in structures *a*, *b*, *c*, and *e* by simply counting the bright spots within the respective unit cells.

We count 20 Pd atoms in the unit cell for structure *a* and 19 for structure *b*. Regarding the positions of Pd, the only difference between *a* and *b* is that we observe two Pd atoms appearing exceptionally bright in *a*, whereas only a single atom is visible in structure *b*. Four additional spots of moderate brightness cannot be clearly attributed to Pd. We will show in Sec. IV B. that these atoms are oxygen. The number of Pd atoms in structure *c* can be determined as 23 in a similar way.

Figure 2 shows that the long chains in structure *e* consist of segments, which are about 0.3 nm long and contain two Pd atoms. For short chains, such as in structure *d*, a finite number of similar segments is added to the $\sqrt{6}$ structure. Therefore, the number of Pd atoms in these unit cells is two times the number of added segments plus five Pd atoms from the Pd_5O_4 cell.

D. Determining the O positions

Since exactly the same surface oxides form on a Pd(111) single crystal surface as on a 3-ML thin Pd layer grown on a partly reduced Rh(111) oxide, we conclude that the maximum oxide thickness must not exceed a few monolayers. Similarities in appearance with Pd_5O_4 as well as only slight atomic displacements in transition regions from the new oxides to Pd_5O_4 (see Fig. 2) indicate oxide structures of single layer thickness.

In our STM images, only Pd is displayed bright, whereas O is dark in most cases. To determine the oxygen positions, we rely on the different appearance of Pd atoms, which depends on their local O coordination.[4,13] In images with moderate resolution, such as Figs. 1(a) and 1(b), Pd atoms with twofold O coordination appear blurred and blend into lines, whereas Pd with four O neighbors appears more distinctly as single atoms. Regarding the position of the oxide layer on the substrate, we assume that O tends to avoid hollow positions of the substrate, as for many surface oxides.[4–6,9,12,13]

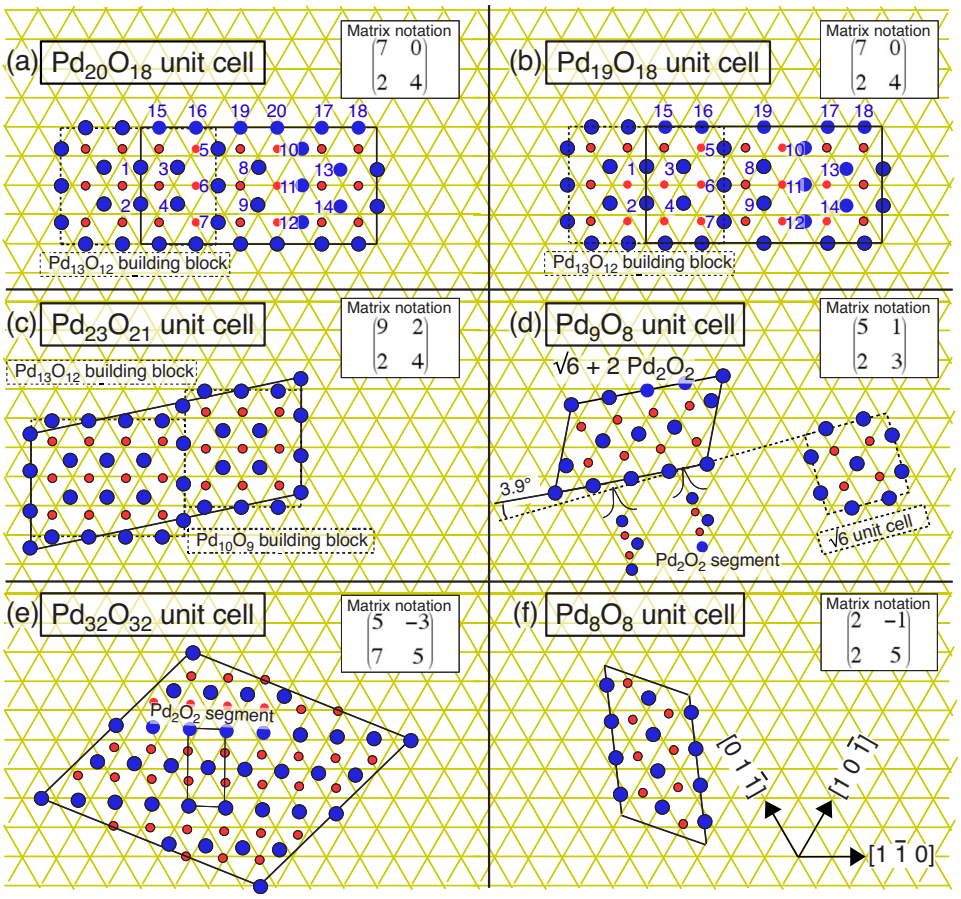

FIG. 4. (Color online) One-layer surface oxide structures as determined from STM. In the oxide layer, Pd atoms are indicated by large (blue) circles, O by small (red) circles, and the topmost substrate Pd(111) layer is indicated by lines with Pd at crossing points.

We placed 20 (19) Pd atoms in the commensurate unit cell of structure *a* (*b*) according to Sec. III C. These atoms are numbered in Figs. 4(a) and 4(b). Since Pd atoms 1, 2, 3, 4, 13, and 14 appear bright and sharp in Fig. 1(a), they are fourfold oxygen coordinated. Therefore, the as-yet undetermined bright spots sometimes appearing in STM images (Fig. 2) are oxygen. Pd atoms 15, 16, 17, and 18 at the border of the unit cell appear blurred in Fig. 1(a), as do atoms 5, 6, 7, 10, 11, and 12, which thus have to be twofold oxygen coordinated. This determines all oxygen positions. As indicated in Figs. 4(a) and 4(b), structures *a* and *b* consist of $Pd_{13}O_{12}$ building blocks separated by transition structures so as to achieve commensurability. Oxygen atoms form a rectangular lattice with only twofold- or fourfold-oxygen-coordinated Pd atoms and quite similar atomic distances as for Pd_5O_4.[4] The oxygen arrangement is similar for both structures *a* and *b*, except for some small local relaxations, which were found by DFT (Sec. IV). Therefore, the stoichiometries of structures *a* and *b* are $Pd_{20}O_{18}$ and $Pd_{19}O_{18}$, respectively. The only difference between these two structures is the Pd arrangement (atom 19 vs 19 and 20) in the transition structure between two $Pd_{13}O_{12}$ building blocks, mentioned already in the previous section. What remains to be done is to arrange the unit cell correctly with respect to the substrate to minimize the number of O atoms in unfavorable hollow positions. The resulting arrangement is displayed in Figs. 4(a) and 4(b). Regarding the Pd positions in $Pd_{20}O_{18}$, we see in Fig. 4(a) that the two Pd atoms (Nos. 19 and 20) appearing exceptionally bright in STM are located very close to on-top positions. Since these two atoms are the only Pd atoms in the unit cell (and in any other surface oxide structure discussed in this paper) sitting close to on-top positions, this uncommon arrangement explains their exceptional brightness. The single bridge-site Pd that replaces these two on-top Pd atoms in $Pd_{19}O_{18}$ [see Fig. 4(b)] does not appear exceptionally bright in STM.

Since structure *c* is composed of the similar $Pd_{10}O_9$ [see Fig. 4(c)] and $Pd_{13}O_{12}$ building blocks, we can place the oxygen atoms and align the structure in the same way as we did for structures *a* and *b*. Adjacent blocks are shifted by a single substrate row distance. Therefore, the stoichiometry of structure *c* is $Pd_{23}O_{21}$ and the model can be seen in Fig. 4(c). Furthermore, as indicated in Fig. 4(c), any sequence of $Pd_{10}O_9$ and $Pd_{13}O_{12}$ building blocks, shifted by one substrate row, forms commensurate structures.

There is a straightforward structural model for adding segments to Pd_5O_4 in order to form rectangular structures with short sides similar to the Pd_5O_4 unit cell (structure *d*). The added segments have a stoichiometry of Pd_2O_2 and the same structure as the segments of the $(\sqrt{5}\times\sqrt{5})R27°$ PdO surface oxide on Pd(100).[5,13] Adding two of these Pd_2O_2 segments to Pd_5O_4, leads to a Pd_9O_8 cell, as displayed in Fig. 4(d). Its structure is thus a combination of the $(\sqrt{5}\times\sqrt{5})R27°$ PdO unit cell in the center and the Pd_5O_4 cell at its short sides. By simply adding Pd_2O_2 segments to Pd_5O_4, one loses commensurability in the $[1\bar{2}1]$ direction. To restore commensurability, the structure is oriented slightly differently with respect to the substrate than the Pd_5O_4 cell. The

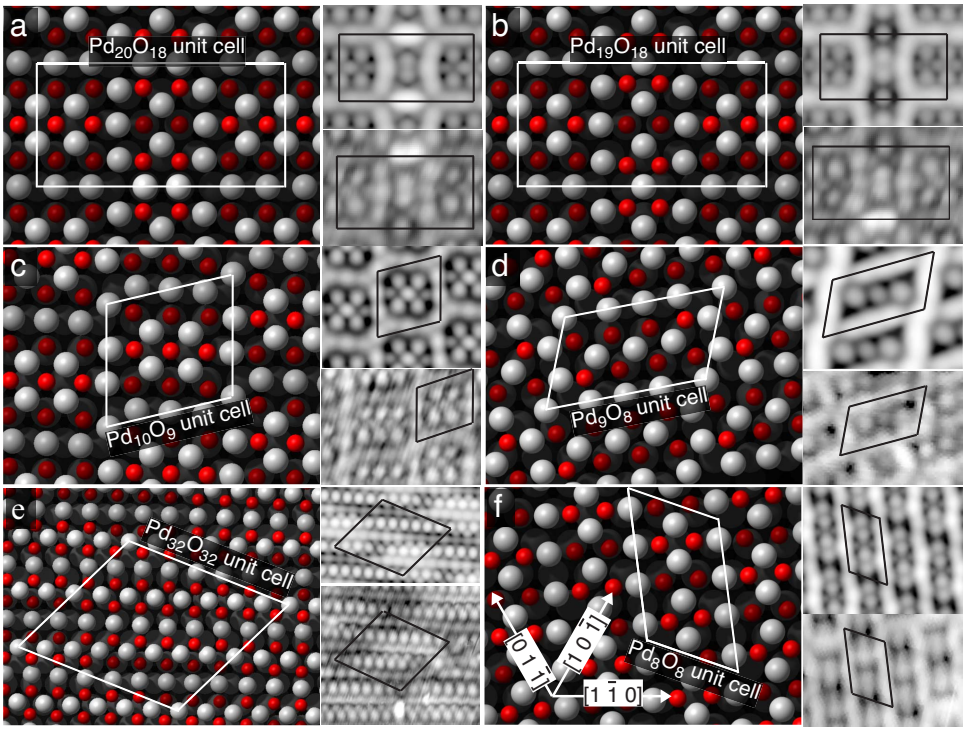

FIG. 5. (Color online) Calculated structure models (left) of (a) $Pd_{20}O_{18}$, (b) $Pd_{19}O_{18}$, (c) $Pd_{10}O_9$, (d) Pd_9O_8, (e) $Pd_{32}O_{32}$, and (f) Pd_8O_8. Oxygen atoms are shown as smaller and darker (red) balls. The buckling of the surface layer in the structure models is indicated by the atom brightness. Simulated and measured STM images are shown at the top and bottom of the right sides, respectively. The experimental STM images in (a) and (b) show the transition between $Pd_{20}O_{18}$ and $Pd_{19}O_{18}$; thus, only the upper side of the unit cell corresponds to the calculation.

alignment of the unit cell with respect to the substrate as displayed in Fig. 4(d) ensures that oxygen is not located in unfavorable hollow positions and Pd is not located on-top of substrate atoms. The calculated rotation of the unit cell compared to Pd_5O_4 for the model in Fig. 4(d) is 3.9°, in perfect agreement with STM [see Fig. 1(b)]. Three Pd atoms in the center of the unit cell of Pd_9O_8 in Fig. 4(d) are fourfold oxygen coordinated and therefore appear as sharp bright dots in STM. Pd atoms at the edge of the unit cell are twofold oxygen coordinated, resulting in a bright blurred seam as observed in Fig. 1(b), assuming a similar brightness contrast as for Pd_5O_4.

As more Pd_2O_2 segments are added, chains are formed which approach PdO stoichiometry. The smallest building block of chains of infinite length is the Pd_2O_2 segment. So half of the Pd atoms in long chains are twofold oxygen coordinated; the other half is fourfold coordinated. This explains why every other Pd row of the chainlike structure *e* appears at a different STM contrast in Fig. 2. A commensurate cell can be obtained by rotating the atom rows 2.8° off a close-packed substrate row [see Fig. 4(e)] leading to a $Pd_{32}O_{32}$ cell. This rotation of the cell avoids on-top positions for twofold Pd. The structure is closely related to the $(\sqrt{5}\times\sqrt{5})R27°$ PdO/Pd(100).[5,13] Along the chains, atom distances are slightly contracted compared to 0.305 nm in $(\sqrt{5}\times\sqrt{5})R27°$ PdO/Pd(100) (taking the domain boundaries into account; see Ref. 13) to an average value of 0.301 nm. Perpendicular to the chains, the in-plane distance between twofold-coordinated Pd is expanded compared to 0.615 nm in $(\sqrt{5}\times\sqrt{5})R27°$ PdO/Pd(100) to 0.63 nm. Nevertheless, this value is less than the width of the Pd_5O_4 unit cell (0.674 nm). The observed wavelike appearance of long PdO chains is necessary to shift certain atoms to more favorable positions on the hexagonal Pd(111) substrate.

Although we could not obtain atomic resolution of Pd for structure *f* in Fig. 1(a), we can set up a structural model by comparison with the other surface oxides. In STM, it appears to be similar to the transition structure between two $Pd_{13}O_{12}$ blocks in $Pd_{19}O_{18}$ [see Fig. 4(b)], although it is rotated by 6.6° to achieve commensurability. This similarity suggests alternating twofold and fourfold Pd atoms, a model similar to the Pd_2O_2 chains of structure *e*, but rotated by roughly 90° [see Fig. 4(f)]. The different orientation with respect to the substrate leads to slightly different atomic distances: 0.300 nm along the rows and 0.663 nm between rows of twofold Pd.

IV. COMPUTATIONAL RESULTS

Approximate atomic positions of O and Pd within the oxide plane and the unit cells of the oxide structures have been determined from STM in Sec. III. These in-plane data are taken as input parameters for DFT calculations in order to obtain detailed structural data and to assess the stability of the structures and to obtain detailed atomic positions. STM images were calculated in order to have a direct comparison with experimental images. Since all STM images in Figs. 1 and 2 were taken close to Fermi energy, an energy range of 0.2 eV below and above Fermi level was used to calculate images, employing the Tersoff-Hamann approach[24] (see Fig. 5).

A. Structural relaxation

The DFT calculations show buckling of oxygen atoms as indicated by the brightness of atoms in the structure models of Fig. 5. Oxygen in on-top positions is bound to the substrate and therefore sits lower, in agreement with Refs. 4 and 13. On the other hand, buckling of Pd is weak, except for

$Pd_{32}O_{32}$, where the Pd atoms have a clear height modulation [see Fig. 5(e)], and for $Pd_{20}O_{18}$ [see Fig. 5(a)], where two twofold-oxygen-coordinated Pd atoms are located almost on-top and thus shift 28 pm up. Slight in-plane relaxations of certain atoms are also found in our DFT calculations. Oxygen atoms buckling towards the substrate preferably move towards on-top positions of the substrate (e.g., Pd_9O_8 in Fig. 5) as was also observed in Refs. 4 and 13. This confirms the building principles used to align the oxide unit cells with the substrate; i.e., O avoids hollow sites. In-plane relaxation for Pd is weak; only twofold-coordinated Pd slightly relaxes towards the upper oxygen atoms.

B. Simulated vs measured STM

The calculations show excellent agreement between the measured and simulated STM images (Fig. 5). DFT calculations also prove that our assumption in Sec. III C, attributing four moderately bright spots in the $Pd_{13}O_{12}$ building blocks of structures *a*, *b*, and *c* to oxygen, was correct. In the simulated STM images, these four oxygen atoms are the only oxygen atoms that appear almost as bright as fourfold-coordinated Pd. Perfect agreement between simulation and experiment is also observed for $Pd_{20}O_{18}$, where two Pd atoms close to on-top positions of the substrate appear exceptionally bright. Since $Pd_{23}O_{21}$ and its $Pd_{13}O_{12}$ and $Pd_{10}O_9$ building blocks form very similar commensurate oxides, only the simplest $Pd_{10}O_9$ structure was calculated.

The structures containing a variable number of Pd_2O_2 segments are shown in Fig. 5(d) (Pd_9O_8), Fig. 5(e) ($Pd_{32}O_{32}$), and Fig. 5(f) (Pd_8O_8). In the first case, two Pd_2O_2 segments have been added to Pd_5O_4, whereas $Pd_{32}O_{32}$ and Pd_8O_8 represent the case of infinitely long chains. All these results confirm the previous findings that twofold-oxygen-coordinated Pd appears bright and blurred, whereas fourfold-coordinated Pd is bright and sharp. The slight blurring of the fourfold Pd atoms in the experimental image of Fig. 5(f) is attributed to an imperfect STM tip; nevertheless, the pairing of these atoms and the overall height contrast are well reproduced.

C. Stability of the structures

Finally, the stability of all calculated structures $Pd_{20}O_{18}$, $Pd_{19}O_{18}$, $Pd_{10}O_9$ (the simplest of the $Pd_{23}O_{21}$-like structures), Pd_9O_8, $Pd_{32}O_{32}$, and Pd_8O_8 has been determined by means of first-principles thermodynamics, together with that of the "$\sqrt{6}$" surface oxide and the adatom structure at 0.25 ML coverage (Fig. 6). All proposed new surface oxide structures are less stable than Pd_5O_4 under the experimental preparation conditions, indicating that these structures are only metastable. It must be underlined, however, that *ab initio* thermodynamics calculations of surface free energies are expected to posses errors in the order of ~ 10 meV/Å^2—i.e., $\sim 50-100$ meV per (1×1) cell in our case[25]—since only the entropy of oxygen atoms in the gas phase is considered, whereas contributions of the vibrational entropy of surface-bound oxygen to the surface free energies is neglected. As the proposed surface oxides contain approximately 2.6 times more oxygen than the $p(2\times2)$ adatom structure, their vibrational entropy is higher, leading to an overestimate of their free energy; i.e., their stability compared to the adatom phase is underestimated. An energy difference of $\sim 50-100$ meV per (1×1) cell is comparable to energy differences between the energetically least favorable Pd_8O_8 structure and the $p(2\times2)$ at an oxygen chemical potential of -1 eV, as shown in Fig. 6. Since the chemical potential of oxygen is higher at lower temperatures, the formation of the metastable surface oxides proposed in this work might also be enhanced by heating to the target temperature in oxygen, as was performed in the present work (see Sec. II).

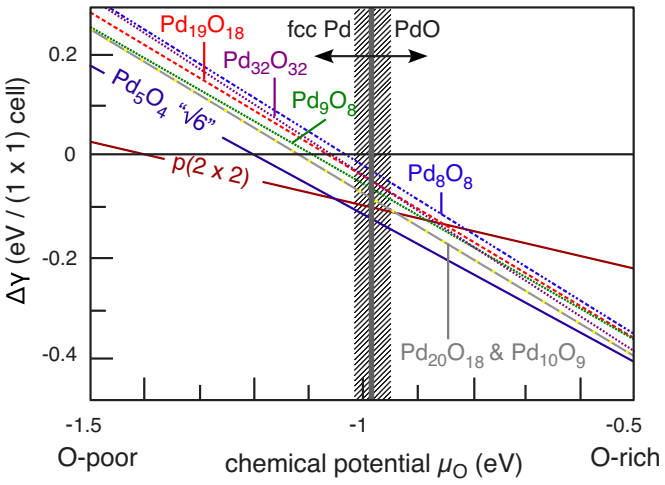

FIG. 6. (Color online) Calculated phase diagram. For each value of the chemical potential, the most stable structure is that represented by the bottommost line. The dashed area indicates preparation conditions. A gray vertical line indicates the border of the PdO stability regime above -1 eV. $\Delta\gamma$ is the difference of surface energy between a given structure and the Pd(111) surface [$\gamma_{Pd(111)} = 0.57$ eV/(1×1) cell].

V. DISCUSSION

A. Building principles

Now that we have found models for the surface oxide structures, we can show that these surface oxides have remarkable structural similarities and simple building rules can be applied. For all of the structures, oxygen forms a rectangular lattice on the hexagonal Pd(111) substrate. The distance between adjacent oxygen atoms in the rectangular lattice is close to the values observed for Pd_5O_4 (Ref. 4) and $(\sqrt{5}\times\sqrt{5})R27°$ PdO/Pd(100).[13] These O-O nearest-neighbor distances, which depend on Pd coordination, rarely lie below 0.3 nm, a value typical for many oxides. Thus, the one-layer surface oxide structures on Pd(111) are strongly determined by oxygen-oxygen repulsion, which can be alleviated by rows of fourfold Pd shielding the O rows from each other, thereby allowing also O-O distances slightly below 0.3 nm. For example, the distance between the O rows separated by fourfold Pd in $Pd_{32}O_{32}$ is only 0.26 nm. Pd is placed in between the oxygen lattice so that it is either twofold or fourfold oxygen coordinated. In the case of Pd_5O_4 (Ref. 4) as

TABLE I. Surface layer atom densities of Pd(111) and one-layer oxides on Pd(111) as well as $(\sqrt{5}\times\sqrt{5})R27°$ PdO/Pd(100) [the latter taking the domain boundaries (Ref. 13) into account].

Structure	O density (nm^{-2})	Pd density (nm^{-2})	Pd+O density (nm^{-2})
Pd(111)	0	15.3	15.3
Pd_5O_4 "$\sqrt{6}$"	8.8	11.0	19.8
Pd_9O_8 *d*	9.4	10.6	20.0
$Pd_{20}O_{18}$ *a*	9.8	10.9	20.7
$Pd_{23}O_{21}$ *c*	10.0	11.0	21.0
$Pd_{19}O_{18}$ *b*	9.8	10.4	20.2
Pd_8O_8 *f*	10.2	10.2	20.4
$Pd_{32}O_{32}$ *e*	10.6	10.6	21.2
PdO/Pd(100)	10.7	10.7	21.4

well as $(\sqrt{5}\times\sqrt{5})R27°$ PdO/Pd(100),[13] every twofold-coordinated Pd atom has its neighboring oxygen atoms on opposite sites, so that one oxygen atom buckles towards the surface whereas the second buckles up. This rule can be explained by bonding to O via a d_{z^2}-like orbital, similar to the $p(4\times4)$-O structure on Ag(111) (Ref. 27) and bulk Ag_2O (Ref. 28). In the newly found surface oxides, this rule for twofold Pd is sometimes violated (see Fig. 5), giving a possible explanation for their lower stability. The oxide structures are aligned on the substrate in such a way that commensurate structures are formed and unfavorable positions, such as on-top sites for Pd and hollow positions for oxygen, can be avoided for almost all surface atoms. Due to buckling of the O atoms, this rule applies more strictly to the lower O atoms than to the upper ones, which are approximately 0.31 nm above the substrate (core-core) and thus only bind to Pd in the oxide layer.

The density of Pd atoms in the oxide layer is similar for all of the observed structures, including Pd_5O_4 and $(\sqrt{5}\times\sqrt{5})R27°$-PdO/Pd(100), but the oxygen density slightly increases compared to Pd_5O_4; in the $Pd_{32}O_{32}$ structure, it approaches the oxygen density of PdO/Pd(100) (see Table I). A higher oxygen density is in agreement with preparation at oxygen-rich conditions. With increasing O/Pd ratio, the number of twofold-coordinated Pd atoms decreases in favor of fourfold-coordinated Pd. For Pd_5O_4 the ratio of fourfold- and twofold-coordinated Pd is 1:4. There are two ways to increase this ratio.

The first possibility is the formation of rectangular structures with short sides of roughly the Pd_5O_4 unit cell side length by adding Pd_2O_2 segments, as demonstrated in Fig. 4(d). Rotation of the chains with respect to $[1\bar{1}0]$ decreases with increasing number of segments from 15° (the value obtained by simply extending the Pd_5O_4 structure) to 2.8° in the case of infinitely long chains [$Pd_{32}O_{32}$ in Fig. 4(e)]. PdO chains can also run almost perpendicular to close-packed substrate rows, as observed for Pd_8O_8 [Fig. 4(f)]. The width of the unit cell changes slightly to adapt to the substrate, and oxygen distances slightly differ from the case of alignment almost parallel to close-packed rows. Regarding surface layer atom densities (Table I), Pd_8O_8 differs more from $(\sqrt{5}\times\sqrt{5})R27°$ PdO/Pd(100) than $Pd_{32}O_{32}$. Furthermore, Pd_8O_8 is thermodynamically the least stable structure at preparation conditions (see Fig. 6) and was only observed in small areas mainly as a transition between strongly misaligned structures such as Pd_5O_4 and $Pd_{20}O_{18}$.

The second possibility to increase the number of fourfold-coordinated Pd is the formation of structures that have two successive fourfold Pd rows followed by one row of twofold Pd ($Pd_{20}O_{18}$, $Pd_{19}O_{18}$, $Pd_{23}O_{21}$). The resulting periodicity of 0.953 nm fits four distances between close-packed Pd rows of the substrate, and all building blocks are aligned parallel to close-packed substrate rows as observed by STM. Since the central oxygen row in each building block lies exactly on a Pd substrate row, its O atoms are in favorable sites. Also the neighboring Pd rows and the other O rows avoid completely unfavorable positions on the substrate. The rows of twofold Pd atoms at the upper and lower sides of the cells [see Figs. 4(a)–4(c)] are in bridge positions at best, forcing the structure to become interrupted regularly to avoid even less favorable sites. This results in the formation of transition structures between the building blocks as for $Pd_{20}O_{18}$ and $Pd_{19}O_{18}$ or in shifting adjacent blocks by one substrate row as for $Pd_{23}O_{21}$ and $Pd_{10}O_9$. Without these interruptions, also some O atoms would be forced to unfavorable positions.

B. Thermodynamic stability

Surprisingly, all proposed structures are energetically significantly less stable than Pd_5O_4 for the preparation conditions used at an oxygen chemical potential of approximately −1 eV (see Fig. 6). In equilibrium, this rules out the possibility of a transition from Pd_5O_4 to bulklike PdO via the observed one-layer oxides with increasing oxygen chemical potential. For Pd(100), it was reported that transition to the bulk oxide occurs through a poorly ordered bulkoxide-like phase, which requires decomposition of the $(\sqrt{5}\times\sqrt{5})R27°$ PdO/Pd(100) surface oxide structure and is kinetically hindered below 675 K.[29] A similar initialization of bulk oxidation might be expected for Pd(111) as well, excluding any of the seven surface oxides on Pd(111) as the precursor of bulk oxidation.

We have to conclude that all observed structures are only kinetically stabilized both towards formation of Pd_5O_4 and towards bulk PdO, which is the most stable structure at preparation conditions above −1 eV (see Fig. 6). There is

also experimental evidence that all observed surface oxide structures are only metastable. Islands on the surface that were formed by excess Pd during oxidation support a kinetic stabilization model, since these islands mostly consist of Pd_5O_4, whereas the terraces are covered by various surface oxides (see Fig. 3). Similarly, it has been observed previously[3] that peninsulas formed by excess Pd consist mainly of Pd_5O_4. This indicates that mobile species, such as Pd expelled during oxidation, form mostly Pd_5O_4, the thermodynamically stable surface oxide, while formation of bulk PdO is still kinetically hindered. Purely kinetic stabilization of a surface oxide has been found also for Rh(111).[6] Kinetic limitations for Pd(111) oxidation have been observed previously,[10] even above the temperatures used in the current study. Unfortunately, an increase of preparation temperature with a simultaneous pressure increase, so as to keep the chemical potential during preparation constant and to avoid kinetic limitations, is beyond the capability of our UHV system.

C. Kinetics of the oxidation

As far as stabilization of the surface oxide structures is concerned, we propose a kinetic explanation, which is based on minimizing the effort for Pd displacements. For the thermodynamically most stable surface oxide structure, Pd_5O_4, there is a substantial rearrangement of the oxide layer Pd atoms compared to the Pd(111) substrate. The angle between the quadratic unit cells and close-packed substrate directions is 15° and the Pd arrangement is far from being hexagonal. Thus, many Pd atoms have to be simultaneously displaced during oxide formation. This can be compared to an infinite PdO chain [$Pd_{32}O_{32}$ model in Fig. 5(e)], which runs almost parallel to a close-packed substrate row and has a quasihexagonal Pd arrangement. Along the chains the Pd in-plane distance is expanded from 0.275 nm to approximately 0.301 nm, perpendicular to the rows the quasihexagonal side length is approximately 0.33 nm. Regarding structures *a*, *b*, and *c*, removing one out of four substrate Pd rows together with a slight expansion of the distances between the remaining Pd atoms results in a quasihexagonal Pd distribution as observed in the center of $Pd_{10}O_9$ and $Pd_{13}O_{12}$ building blocks [see Figs. 4(a)–4(c)]. This scenario can be summarized as two main mechanisms responsible for surface oxide formation: (i) expansion of the Pd lattice leading to the quasihexagonal $Pd_{32}O_{32}$ structure and (ii) a zipperlike mechanism of expelling Pd rows, leading to the $Pd_{10}O_9$ and $Pd_{13}O_{12}$ building blocks. So we can argue that an arrangement of the surface oxide layer parallel to a close-packed substrate direction as well as a quasihexagonal Pd arrangement minimizes the kinetic effort during oxide formation. On the other hand, the short chains in Pd_9O_8 as well as the chains in Pd_8O_8 do not run parallel to the substrate. These structures are only observed in small areas as a transition between other surface oxides. We consider it possible that these structures form due to in-plane stress leading to local rotation of the lattice when adjacent areas expand due to oxidation.

D. Previous reports on these surface oxides

Similar surface oxides have been observed in Refs. 3 and 10. We can clearly attribute the so-called "wavelike pattern" in Fig. 4(a) of Ref. 10 to a $Pd_{23}O_{21}$-like phase and identify a $Pd_{32}O_{32}$-like phase in the lower part of Fig. 4(b) in Ref. 10. In Ref. 10, preparation was done at a similar temperature of 573 K, but at lower oxygen pressures (by a factor of 100) compared to this work, corresponding to a chemical potential of $\mu_O = -1.05$ eV. According to the phase diagram in Fig. 6, none of the surface oxides *a*–*f* discussed in this work should be stable under these conditions. The cooling process in oxygen used in Ref. 10 can, however, explain $Pd_{32}O_{32}$ and $Pd_{23}O_{21}$ oxide formation, since μ_O increases with decreasing temperature. Oxidation during cooldown again indicates kinetics favoring the formation of these two structures (see Sec. V C) and also explains the coexistence of these oxide phases with the $p(2\times2)$ O-adatom structure. $Pd_{23}O_{21}$- and $Pd_{32}O_{32}$-like phases can also be found in Fig. 8(c) of Ref. 3, though clear similarities become only apparent by comparison with the respective structures *c* and *e* in Fig. 3 (this work). The lattice constant of 0.638 nm as determined from Fig. 8(d) in Ref. 3 for the distance perpendicular to the Pd rows in $Pd_{32}O_{32}$ is in good agreement with our observations (0.626 nm). Although the very weak modulation along the Pd rows (0.394 nm) noted in Ref. 3 is probably unrelated to the lattice constant (0.301 nm in this work), we can safely assume that the same structures were observed in Ref. 3 and in the present work.

VI. SUMMARY

Oxidation of the Pd(111) surface has been studied by STM and DFT at preparation temperatures of 570–605 K and oxygen-rich conditions, corresponding to an oxygen chemical potential above −1 eV, which is already in the stability regime of the PdO bulk oxide. Since the Pd(111) surface is covered by small domains of various surface oxides, STM is the adequate experimental method for determining local structures. In addition, DFT calculations were used to simulate STM images as well as to determine the stability of the surface oxide structures. Structural details of six one-layer surface oxides on Pd(111) are reported in this paper: namely, Pd_9O_8, $Pd_{20}O_{18}$, $Pd_{23}O_{21}$, $Pd_{19}O_{18}$, Pd_8O_8, and $Pd_{32}O_{32}$. All oxide structures are driven by the requirement to have a favorable alignment of the oxide layer with respect to the substrate. Structural similarities to Pd_5O_4/Pd(111) and $(\sqrt{5}\times\sqrt{5})R27°$ PdO/Pd(100) were observed. An increase of the oxygen concentration compared to Pd_5O_4, approaching PdO stoichiometry and reflecting preparation at oxygen rich conditions, has been found. Since all oxides considered in this paper are thermodynamically less stable than Pd_5O_4 at preparation conditions, we have argued that these structures are kinetically stabilized and discussed possible mechanisms for their formation.

ACKNOWLEDGMENTS

This work was financially supported by the Austrian Fonds zur Förderung der wissenschaftlichen Forschung and the European Union under Contract No. NMP3-CT-2003-505670 (NANO2).

*Corresponding author. schmid@iap.tuwien.ac.at

[1] H. Over, Y. D. Kim, A. P. Seitsonen, S. Wendt, E. Lundgren, M. Schmid, P. Varga, A. Morgante, and G. Ertl, Science **287**, 1474 (2000).
[2] B. L. M. Hendriksen and J. W. M. Frenken, Phys. Rev. Lett. **89**, 046101 (2002).
[3] G. Zheng and E. I. Altman, Surf. Sci. **462**, 151 (2000).
[4] E. Lundgren, G. Kresse, C. Klein, M. Borg, J. N. Andersen, M. De Santis, Y. Gauthier, C. Konvicka, M. Schmid, and P. Varga, Phys. Rev. Lett. **88**, 246103 (2002).
[5] M. Todorova, E. Lundgren, V. Blum, A. Mikkelsen, S. Gray, J. Gustafson, M. Borg, J. Rogal, K. Reuter, J. N. Andersen, and M. Scheffler, Surf. Sci. **541**, 101 (2003).
[6] J. Gustafson, A. Mikkelsen, M. Borg, E. Lundgren, L. Köhler, G. Kresse, M. Schmid, P. Varga, J. Yuhara, X. Torrelles, C. Quirós, and J. N. Andersen, Phys. Rev. Lett. **92**, 126102 (2004).
[7] K. Reuter and M. Scheffler, Appl. Phys. A: Mater. Sci. Process. **78**, 793 (2004).
[8] G. Kresse, M. Schmid, E. Napetschnig, M. Shishkin, L. Köhler, and P. Varga, Science **308**, 1440 (2005).
[9] J. Gustafson, A. Mikkelsen, M. Borg, J. N. Andersen, E. Lundgren, C. Klein, W. Hofer, M. Schmid, P. Varga, L. Köhler, G. Kresse, N. Kasper, A. Stierle, and H. Dosch, Phys. Rev. B **71**, 115442 (2005).
[10] H. Gabasch, W. Unterberger, K. Hayek, B. Klötzer, G. Kresse, C. Klein, M. Schmid, and P. Varga, Surf. Sci. **600**, 205 (2006).
[11] C. Dri, C. Africh, F. Esch, G. Comelli, O. Dubay, L. Köhler, F. Mittendorfer, G. Kresse, P. Dudin, and M. Kiskinova, J. Chem. Phys. **125**, 094701 (2006).
[12] E. Lundgren, A. Mikkelsen, J. N. Andersen, G. Kresse, M. Schmid, and P. Varga, J. Phys.: Condens. Matter **18**, R481 (2006).
[13] P. Kostelník, N. Seriani, G. Kresse, A. Mikkelsen, E. Lundgren, V. Blum, T. Šikola, P. Varga, and M. Schmid, Surf. Sci. **601**, 1574 (2007).
[14] E. Lundgren, J. Gustafson, A. Resta, J. Weissenrieder, A. Mikkelsen, J. N. Andersen, L. Köhler, G. Kresse, J. Klikovits, A. Biedermann, M. Schmid, and P. Varga, J. Electron Spectrosc. Relat. Phenom. **144-147**, 367 (2005).
[15] J. Klikovits, M. Schmid, J. Gustafson, A. Mikkelsen, A. Resta, E. Lundgren, J. N. Andersen, and P. Varga, J. Phys. Chem. B **110**, 9966 (2006).
[16] H. Conrad, G. Ertl, J. Küppers, and E. E. Latta, Surf. Sci. **65**, 245 (1977).
[17] P. Légaré, L. Hilaire, G. Maire, G. Krill, and A. Amamou, Surf. Sci. **107**, 533 (1981).
[18] D. L. Weissman-Wenocur, M. L. Shek, P. M. Stefan, I. Lindau, and W. E. Spicer, Surf. Sci. **127**, 513 (1983).
[19] A. P. Seitsonen, Y. D. Kim, S. Schwegmann, and H. Over, Surf. Sci. **468**, 176 (2000).
[20] G. Kresse and J. Furthmüller, Comput. Mater. Sci. **6**, 15 (1996); Phys. Rev. B **54**, 11169 (1996).
[21] P. E. Blöchl, Phys. Rev. B **50**, 17953 (1994).
[22] G. Kresse and D. Joubert, Phys. Rev. B **59**, 1758 (1998).
[23] J. P. Perdew, J. A. Chevary, S. H. Vosko, K. A. Jackson, M. R. Pederson, D. J. Singh, and C. Fiolhais, Phys. Rev. B **46**, 6671 (1992).
[24] J. Tersoff and D. R. Hamann, Phys. Rev. Lett. **50**, 1998 (1983).
[25] K. Reuter and M. Scheffler, Phys. Rev. B **65**, 035406 (2001); **75**, 049901(E) (2007).
[26] N. Seriani, W. Pompe, and L. C. Ciacchi, J. Phys. Chem. B **110**, 14860 (2006).
[27] M. Schmid, A. Reicho, A. Stierle, I. Costina, J. Klikovits, P. Kostelnik, O. Doubay, G. Kresse, J. Gustafson, E. Lundgren, J. N. Anderson, H. Dosch, and P. Varga, Phys. Rev. Lett. **96**, 146102 (2006).
[28] A. Deb and A. K. Chatterjee, J. Phys.: Condens. Matter **10**, 11719 (1998).
[29] E. Lundgren, J. Gustafson, A. Mikkelsen, J. N. Andersen, A. Stierle, H. Dosch, M. Todorova, J. Rogal, K. Reuter, and M. Scheffler, Phys. Rev. Lett. **92**, 046101 (2004).